# Transient Studies of Oxygen Removal Pathways and Catalytic Redox Cycles during NO Decomposition on Cu−ZSM5

**Björn Modén, Patrick Da Costa, Deuk Ki Lee,† and Enrique Iglesia***

*Department of Chemical Engineering, University of California at Berkeley, Berkeley, California 94720*

*Received: March 15, 2002; In Final Form: June 18, 2002*

The identity of reactive intermediates and of active sites and the details of redox cycles and oxygen removal pathways during NO decomposition on well-characterized Cu−ZSM5 were examined by combining previous spectroscopic and steady-state kinetic studies with measurements of the rate of evolution of NO, $N_2O$, $NO_2$, $N_2$, and $O_2$ during isothermal and nonisothermal kinetic transients. The oxygen coverages measured during reversible isothermal switches from He to NO/He mixtures showed that NO decomposition involves bimolecular reactions of two NO molecules adsorbed on vicinal $Cu^+$ species with the formation of $N_2O$ as the initial product near ambient temperature. These vicinal $Cu^+$ species form via oxygen removal from $\{Cu^{2+}-O^{2-}-Cu^{2+}\}^{2+}$ to form $\{Cu^+-\square-Cu^+\}^{2+}$ using $NO_2$ as an oxygen carrier among distant oxidized dimers. Adsorbed nitrate ($NO_3$*) is the kinetically relevant intermediate in the formation of $O_2$ during NO decomposition. This $NO_3$* decomposition reaction is one of the steps involved in the equilibrated formation of $NO_2$ observed during NO decomposition. These NO-mediated oxygen removal pathways, in which NO acts both as a reductant and as an oxidant, are significantly more rapid than recombinative desorption steps. The desorption of products and of unreacted NO during reactions of preadsorbed NO with increasing catalyst temperature confirmed the bimolecular nature and the low activation energy for $N_2O$ formation from NO. The facile nature of this reaction and the unfavorable NO adsorption thermodynamics as temperature increases combine to give the observed decrease in NO decomposition rates at high temperatures. These findings are consistent with some reported mechanism-based steady-state rate expressions and with previous infrared detection of the reaction intermediates proposed here based on isothermal and nonisothermal transients. These pathways appear to be relevant also to $N_2O$ decomposition reactions, which occur after the initial formation of $N_2O$ from NO and involve reactions of $N_2O$ with $\{Cu^+-\square-Cu^+\}^{2+}$ and removal of oxygen via NO-mediated desorption pathways. This study brings consensus and some clarification into the mechanistic details for NO and $N_2O$ decomposition reactions and resolves some remaining discrepancies and some contradictory conclusions in previous reports.

## Introduction

Direct decomposition of NO to $N_2$ and $O_2$ remains potentially attractive for $NO_x$ removal from combustion streams because reaction thermodynamics are favorable and no sacrificial reductants are required. Catalytic NO decomposition rates, however, are currently too low for practical use. Cu-exchanged ZSM5 zeolites are among the most active NO decomposition catalysts.[1−5] Several studies have addressed the reaction pathways leading to N−N and O−O bond formation during NO decomposition on Cu−ZSM5.[6−26]

Cu is present in Cu−ZSM5 as divalent cations after exchange and thermal treatment in air. The predominant Cu species are isolated $Cu^{2+}$ cations and $\{Cu^{2+}-O^{2-}-Cu^{2+}\}^{2+}$ dimers, each interacting with two exchange sites.[27] CuO particles can also form in these samples, depending on the synthesis method,[6] but they were not detected in the samples used in the present study. Cu dimers have been proposed as the active species in NO decomposition.[5−7] In contrast with isolated $Cu^{2+}$ cations, these dimers contain a removable oxygen atom; as a result, they can undergo the redox cycles implicated in NO decomposition turnovers.

We have previously reported steady-state kinetic rate data for NO decomposition and a consistent set of elementary steps.[26] These elementary steps replace previously proposed oxygen removal pathways, which require recombinative desorption of nonvicinal oxygens, with a catalytic $NO-NO_2$ cycle that forms $O_2$ using oxygen atoms in nonvicinal $\{Cu^{2+}-O^{2-}-Cu^{2+}\}^{2+}$ dimers. This catalytic sequence accounts for the unusual decrease in NO decomposition rates observed above 773 K.[3,8,26] At lower temperatures, $O_2$ inhibits NO decomposition rates because of competitive adsorption of oxygen and NO on reduced $Cu^+$ sites. This inhibition leads to the normal Arrhenius behavior prevalent below 773 K. At these temperatures, $O_2$ inhibition effects become less severe, $\{Cu^+-\square-Cu^+\}^{2+}$ species become the most abundant surface intermediates, and the adsorption of NO on such species becomes thermodynamically unfavored. This leads to the decrease in NO decomposition rates observed at higher temperatures.

Isothermal transient studies of NO decomposition on Cu−ZSM5 have been previously reported.[9−12] In these measurements, an inert flow is replaced with a stream containing NO. $N_2$ formation rates are initially high, but they decrease as the system approaches steady state.[9−11] $O_2$ evolution rates are

* To whom correspondence should be addressed. Telephone: (510) 642-9673. Fax: (510) 642-4778. E-mail: iglesia@cchem.berkeley.edu.

† Permanent address: Division of Civil and Environmental Engineering, Kwangju University, Kwangju 503-703, Korea.

10.1021/jp020731g CCC: $22.00 
Published on Web 08/27/2002

**TABLE 1: Elemental Composition and Cu Speciation**

| | Cu(0.36)[a] | Cu(0.58) | Cu(0.60) |
|---|---|---|---|
| Cu (wt %) | 2.25 | 3.31 | 3.88 |
| Si/Al | 14.0 | 15.0 | 14.0 |
| $Cu_{dimer}/Cu_{total}$[b] | 0.56 | 0.70 | 0.78 |

[a] Atomic Cu/Al ratio. [b] Measured from the $CO_2$ produced during CO-TPR after $O_2$ treatment.[27]

initially lower than $N_2$ formation rates, but they increase to the equimolar reaction stoichiometry at steady state. The subsequent removal of NO from an inert stream leads to initial $O_2$ evolution rates exceeding those measured during steady-state NO decomposition. This has led to the proposal that NO stabilizes adsorbed oxygen in the form of a $Cu^{2+}(O)(NO)(NO_2)$ species.[11]

In situ infrared studies coupled with mass spectrometry have been used to detect adsorbed species during isothermal NO transients.[12] The introduction of NO at 673 K led to the immediate appearance of a band assigned to $Cu^+(NO)$, and then to a band for bridging $Cu^{2+}-(NO_3^-)-Cu^{2+}$.[12] These were the only infrared bands detected at 673 K. Infrared studies have also confirmed that NO adsorbs on $Cu^+$ [5,13−18] and suggested that $Cu^+/Cu^{2+}$ redox reactions occur as conditions change from reducing to oxidizing.[19]

NO decomposition appears to occur via the initial formation of $N_2O$ followed by its decomposition.[26] $N_2O$ and small amounts of $N_2$ are typically detected during temperature-programmed desorption of preadsorbed NO on Cu−ZSM5.[10,12,20−23] Two low-temperature $N_2O$ desorption peaks and one $O_2$ evolution peak at higher temperatures have been detected along with broader NO desorption peaks over a wide range of temperature (300−750 K).[20] Oxidation of the sample before NO adsorption markedly decreased the amount of $N_2O$ formed.[20]

Here, we report isothermal and nonisothermal transient experiments carried out in the presence and absence of NO in the carrier gas in order to confirm the details of the elementary steps proposed previously based on steady-state kinetic data.[26] These experiments are then brought together with these steady-state kinetic data and with detailed structural characterization and reduction studies of the Cu species in these materials.[27] We conclude with a model of the site requirements and the mechanism of NO decomposition on Cu−ZSM5.

## Experimental Methods

**Catalyst Synthesis and Characterization.** The synthesis of the Cu−ZSM5 catalysts and the characterization of their structure and reduction properties have been described in detail elsewhere.[27] Elemental analyses are shown in Table 1 for all catalysts used in this study. All samples are denoted as Cu(*x*), where *x* is the atomic Cu/Al ratio. The $Cu_{dimer}/Cu_{total}$ ratio represents the fraction of the total Cu atoms that are present in Cu dimers.

**Reactant and Treatment Gas Mixtures.** The NO-containing stream contained 1.00% NO, 9.98% Ar, and 89.02% He (Matheson; <10 ppm impurities). Ar was included as an internal standard for mass spectrometric analyses. The $O_2$ stream consisted of 50% $O_2$/He (Matheson); it was purified by passing through a 13X molecular sieve at ambient temperature. Helium (UHP, Bay Airgas) was used as a diluent for both $O_2$ and NO streams and as an inert carrier gas in transient and desorption experiments. Helium was purified by passage through a 13X molecular sieve and an oxygen trap (Matheson). The mass spectrometer was calibrated for $N_2$, $O_2$, and $N_2O$ using a mixture containing 0.05% $N_2$, 0.05% $O_2$, 0.05% $N_2O$, 10% Ar, and 89.85% He (Praxair) and for $NO_2$ using another mixture containing 0.05% $NO_2$, 10% Ar, and 89.95% He (Praxair).

**Mass Spectrometric Analysis of Reactant and Product Streams.** Reactants and product streams were analyzed using on-line mass spectrometry (MKS Instruments, Orion Compact Residual Gas Analyzer) and a differentially pumped atmospheric sampling system (Pfeiffer, vacuum system TCP015, turbomolecular pump Model TMU065). He (4 amu), $N_2$ (28 amu), NO (30 amu), $O_2$ (32 amu), Ar (40 amu), $N_2O$ (44 amu), and $NO_2$ (46 amu) were monitored continuously with a time resolution of 2 s for the isothermal transient experiments, for which high time resolution was required, and 10 s for other experiments. In all figures, products detected only in trace amounts are not reported.

**Sample Treatment Protocols.** All Cu−ZSM5 samples in this study were treated in either oxidative or nonoxidative environments before transient experiments. The oxidative treatment consisted of contact with 50% $O_2$/He at 5.33 $cm^3$ (g of catalyst)$^{-1}$ $s^{-1}$ as the temperature was increased at 0.167 K $s^{-1}$ to 773 K. The sample was held at 773 K for 2 h, and was then cooled slowly to ambient temperature. After reaching ambient temperature, the $O_2$/He stream was replaced with 16.7 $cm^3$ (g of catalyst)$^{-1}$ $s^{-1}$ He in order to remove weakly adsorbed $O_2$. Helium was used for the nonoxidative treatment. The flow rates and temperature profile were identical to those for the $O_2$/He treatment, except that He was used as the carrier gas instead of 50% $O_2$/He.

**Isothermal Transients.** Isothermal transient measurements consisted of rapid switches between He and NO-containing streams with various NO concentrations. These experiments were carried out using a system designed to minimize hydrodynamic delays. The mean mixing time for a step change in NO concentration was <10 s at a flow rate of 1.67 $cm^3$ $s^{-1}$.

**Temperature-Programmed Desorption (TPD) Studies.** NO was adsorbed on Cu−ZSM5 (0.3 g) by contacting catalyst samples with 1% NO (1.67 $cm^3$ $s^{-1}$) for 900 s at ambient temperature, after treating the samples in either He or 50% $O_2$/He, as described above. After adsorption, the NO stream was replaced with He (1.67 $cm^3$ $s^{-1}$; 0.5 h) at ambient temperature in order to desorb weakly bound species. The temperature was then increased from ambient temperature to 823 K at 0.167 K $s^{-1}$. Temperature-programmed desorption of adsorbed oxygen was performed by treating the catalyst in 50% $O_2$/He, and then heating at 0.167 K $s^{-1}$ from ambient temperature to 1100 K in 1.67 $cm^3$ $s^{-1}$ He.

**Desorption and Decomposition of Adsorbed NO Using NO-containing Carrier Gas.** NO desorption and decomposition rates were measured on Cu−ZSM5 (Cu/Al = 0.58; 0.3 g) as a function of temperature during continuous NO flow. NO (0.464% NO/He) was introduced at 1.67 $cm^3$ $s^{-1}$ after treatment in 50% $O_2$/He, and the sample temperature was increased to 923 K at 0.167 K $s^{-1}$.

## Results and Discussion

This study attempts to probe mechanistic details of NO decomposition and the nature of the active intermediates and of the sites required for kinetically relevant steps using a combination of isothermal transient and temperature-programmed rate measurements. The various species likely to exist on Cu sites during NO decomposition are shown schematically in Figure 1, where * denotes a reduced Cu dimer $\{Cu^+-\square-Cu^+\}^{2+}$. Nitrate species have been detected by infrared spectroscopy; they appear to be the most stable N-containing adsorbed species on Cu−ZSM5 during NO decomposition.[12,18]

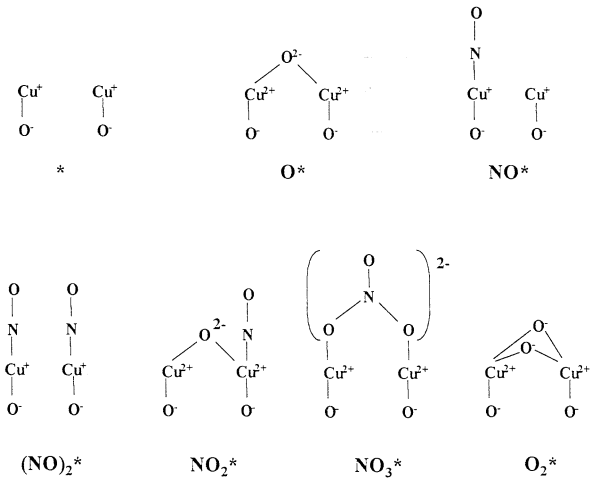


**Figure 1.** Cu dimer species on two Al sites (represented by $O^-$) and adsorbed species proposed to exist on such Cu dimers during catalytic NO decomposition on Cu−ZSM5.

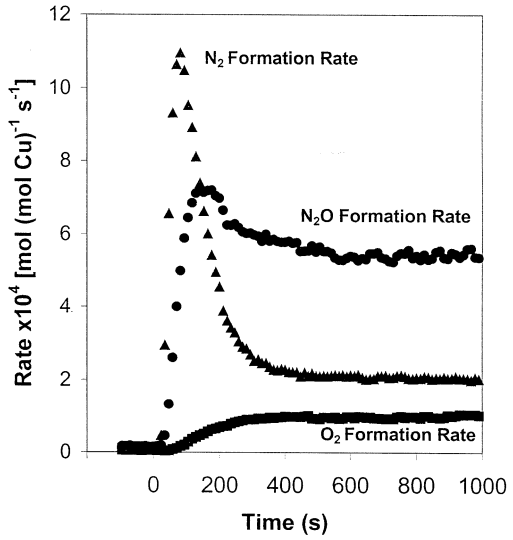


**Figure 2.** $N_2$, $O_2$, and $N_2O$ formation rates during an isothermal switch from pure He to 1% NO at 623 K [Cu(0.36), 0.1 g, 1.67 $cm^3$ $s^{-1}$ total flow rate].

Different forms of adsorbed $NO_3$ and $NO_2$ species have been proposed, but the exact structure of these species is beyond the scope of this study, in which we are concerned only with the stoichiometry and reactivity of such species.

**NO Decomposition during Isothermal Transients.** The evolution of products after a rapid switch from He to NO-containing streams can be used to measure the oxygen content and the concentration of reaction intermediates in each sample as it approaches the catalytic steady state. In contrast with temperature-programmed experiments, in which both the surface coverage of intermediates and the value of the kinetic parameters change during the experiment, only the former varies during isothermal transients.

Isothermal NO decomposition transient data at 623 and 773 K are shown in Figures 2 and 3, respectively. Between these two temperatures, NO decomposition rates change their temperature dependence from their normal increase with temperature to a decrease in rate with increasing temperature above ~723 K; these changes in temperature response are likely to reflect changes in the identity of the most reactive surface intermediates.[28] Thus, it is useful to contrast the catalytic behavior exhibited by Cu−ZSM5 at these two temperatures.

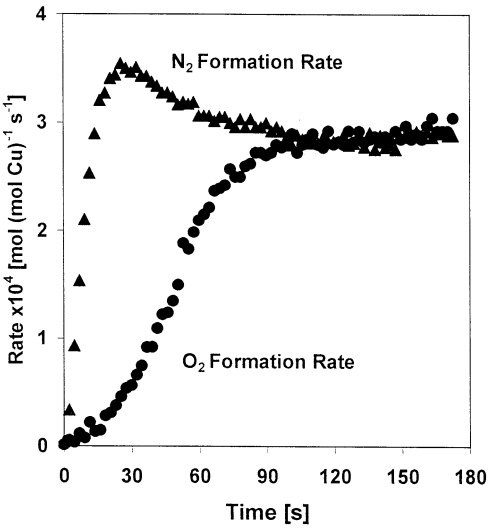


**Figure 3.** $N_2$ and $O_2$ formation rates during an isothermal switch from pure He to 0.464% NO at 773 K [Cu(0.36), 0.1 g, 1.67 $cm^3$ $s^{-1}$ total flow rate].

Below 673 K, $NO_3$* is likely to be present at high surface coverages,[12,18] while O* and * are expected to become the most abundant surface intermediates at higher temperatures. Immediately after the step change from He to NO, $N_2$ and $N_2O$ evolution rates increased sharply and then decreased (Figure 2). The rate of appearance of products with excess N-atoms ($N_2$ and $N_2O$; relative to the equimolar ratio in NO) exceeds that for the formation of products with excess O-atoms ($O_2$ and $NO_2$) (Figures 2 and 3). This imbalance reflects the net retention of oxygen by Cu−ZSM5 during the initial stages of NO decomposition. $N_2$ and, at lower temperatures, $N_2O$ are initially formed at rates higher than their steady-state values. This indicates that the accumulation of oxygen, as O*, $NO_2$*, or $NO_3$*, titrates the active sites required for NO chemisorption and for decomposition turnovers and inhibits the rate of $N_2$ and $N_2O$ formation steps. As the surface oxygen content increases with time elapsed after the switch, the rate of $O_2$ formation concurrently increases and the O and N imbalance ultimately disappears.

At 773 K, the maximum $N_2$ formation rates measured after the switch are closer to their corresponding steady-state values than in similar experiments at 623 K (cf. Figures 2 and 3). This indicates a weaker inhibition of NO decomposition rates by oxygen-rich adsorbed species at higher temperatures. In effect, a smaller amount of surface oxygen is retained by the surface as NO decomposition rates reach steady-state values at 773 K than at 623 K. This is consistent with the lower expected coverages of adsorbed oxygen species [$\Theta_O$, mol of O (mol of Cu)$^{-1}$] at higher temperatures.

The change in surface oxygen coverage during an isothermal transient can be measured from the transient evolution in the rates of product formation. The feed contains equimolar amounts of N and O; therefore, the net rate of oxygen adsorption, $r_{O,ads}$, equals the difference between the rates of appearance of N- and O-atoms among reaction products (eq 1).

$$r_{O,ads} = r_{N,tot} - r_{O,tot} = 2r_{N_2} + r_{N_2O} - 2r_{O_2} - r_{NO_2} \quad (1)$$

The integration of this net oxygen retention rate with time gives the fractional oxygen coverage on the surface, $\Theta_O$. The starting point of this integration was estimated from an $O_2$ TPD (in He) for the catalyst Cu(0.36).[27] During $O_2$ TPD, up to 773 K, ~0.20

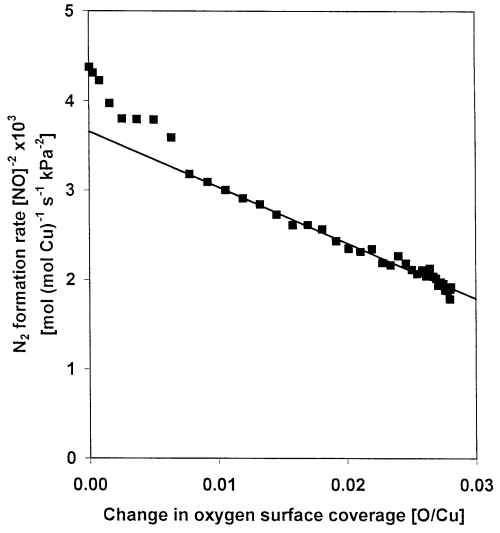


**Figure 4.** $N_2$ formation rate during isothermal switch from pure He to 0.464% NO at 773 K as a function of oxygen surface coverage [mol of O (mol of Cu)$^{-1}$]. The $N_2$ rate is divided by $[NO]^2$ to account for the initial gradual increase in NO concentration caused by the system hydrodynamic delay [Cu(0.36), 0.1 g, 1.67 cm$^3$ s$^{-1}$ total flow rate].

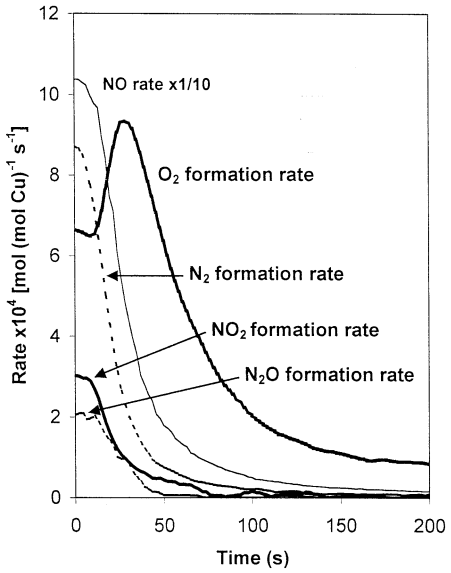


**Figure 5.** $N_2$, $O_2$, $N_2O$, and $NO_2$ formation rates and NO exit rate during an isothermal switch from 1% NO to helium at 673 K [Cu(0.58), 0.1 g, 1.67 cm$^3$ s$^{-1}$ total flow rate].

O/Cu remains adsorbed on the catalyst and provides the initial oxygen content at the point of the He to NO switch.

During the initial part of the transient, the NO partial pressure gradually increased because of short (but measurable) hydrodynamic delays. This must be taken into account in the analysis of the transient kinetic response. The internal standard Ar was used to measure the inlet NO partial pressure during the isothermal transient, and this in turn was used to calculate a rate normalized to the NO partial pressure using a second-order NO dependence, obtained from steady-state kinetics.[26]

The effect of oxygen surface coverage, $\Theta_O$, on $N_2$ formation rates is shown in Figure 4 using the second-order NO concentration correction for the same experiment as in Figure 3. Except for the first few data points, $N_2$ formation rates decreased linearly with increasing $\Theta_O$, as expected from the reaction kinetics (eq 2), the details of which have been discussed elsewhere:[26]

$$\frac{r_{N_2}}{[NO]^2} = k_{app}\frac{[*]}{[L]} = k_{app}\frac{([L] - [O*])}{[L]} = k_{app}(1 - \Theta_O) \quad (2)$$

At 773 K, O* and * appear to be the most abundant surface species, and consistent with this, $NO_x$-adsorbed species have not been detected by infrared spectroscopy at this temperature.[12,18] Thus, an increase in $\Theta_O$ corresponds to a proportional decrease in $\Theta$*. The observed linear decrease in $N_2$ formation rates is consistent with the requirement for reduced Cu centers (*) for NO chemisorption and decomposition steps, as well as the redox nature of NO decomposition catalytic cycles. Previously reported kinetic data[26] showed that the steady-state reaction is second order in NO, but the second-order correction overpredicts the rate during the initial hydrodynamic transient (Figure 4), whereas a correction that assumes a first-order NO dependence significantly underpredicts the rate. This indicates that NO adsorption steps are not fully quasi-equilibrated during the early stages of the transient, leading to an apparent NO reaction order slightly smaller than its steady-state value of two.

After steady-state NO decomposition rates were reached with 1.0% NO reactants at 673 K, a switch to pure He led to initial $O_2$ formation rates significantly higher than at steady state (Figure 5). During the catalytic reaction, $O_2$ formation rates reflect the difference between the forward and the reverse rates of the elementary steps leading to the formation of $O_2$. As a result, an increase in $O_2$ formation rates after NO is removed from the gas phase can arise from either an increase in the forward rate of $O_2$ evolution or from a decrease in the corresponding reverse rate (or from a combination of these two effects). The removal of NO from the gas phase leads to a gradual decrease in the concentration of all NO-derived adsorbed species, including chemisorbed oxygen. Therefore, the forward rate of formation of $O_2$ from any such adsorbed species derived from NO cannot increase after NO is removed from the flowing stream. The higher than steady-state $O_2$ formation rates observed after NO removal must therefore reflect a decrease in the rate of the microscopic reverse of the step that forms $O_2$. The observed increase in the net $O_2$ formation rate requires that a decrease in this reverse rate also occur more rapidly than any corresponding decrease in the forward rate of the $O_2$ formation reaction. If $O_2$ desorbed only via recombinative desorption of O* ($2O^* \leftrightarrow 2^* + O_2$), its microscopic reverse step—the dissociative chemisorption of $O_2$—would actually increase upon the observed increase in the gas-phase $O_2$ concentration. Thus, $O_2$ removal cannot be occurring predominantly via recombinative desorption pathways during steady-state or transient NO decomposition. Instead, it appears that the reverse of the oxygen removal step involves NO, the concentration of which decreases sharply and immediately after the switch. The surface species that form $O_2$ also form NO concurrently, and the concentration of such species during steady-state NO decomposition must be large enough to account for the large excess of oxygen relative to nitrogen that desorbs in the products after removal of NO from the gas phase. $NO_3$* is the likely intermediate in $O_2$ formation during NO decomposition; it has been detected as the most abundant infrared-active adsorbed species at these temperatures.[12,18] These transient experiments provide kinetic evidence for its role as intermediate in $O_2$ formation.

At 773 K and higher temperatures, the rate of $O_2$ formation after removing NO from the gas phase was not above its value at steady state (Figure 6), indicating that the concentration of the adsorbed species responsible for $O_2$ formation is significantly lower than at 673 K. Infrared studies have shown that adsorbed $NO_3$* species disappear above 723 K,[12,18] and * and O* are

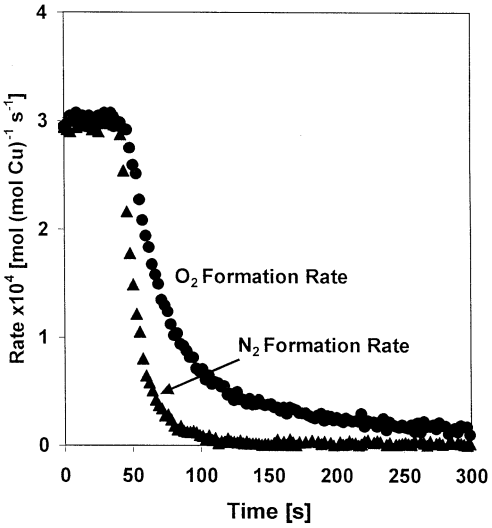


**Figure 6.** $N_2$ and $O_2$ formation rates during an isothermal switch from 0.464% NO to pure He at 773 K. This is a continuation from the experiment in Figure 3 [Cu(0.36), 0.1 g, 1.67 cm$^3$ s$^{-1}$ total flow rate].

expected to become the most abundant reactive intermediates at these temperatures. The low $NO_3$* surface coverages detected at high temperatures are consistent with an exothermic adsorption process, such as $NO_2$ adsorption on oxidized dimers (O*), for which the equilibrium constant decreases with increasing temperature. The absence of detectable $NO_3$* at temperatures above 700 K reflects the stronger temperature dependence for $NO_3$* decomposition relative to its formation, as expected for exothermic reactions. This evidence does not preclude an intermediate role for $NO_3$* in $O_2$ formation during steady-state NO decomposition at these higher temperatures, but only its presence as a detectable reactive intermediate. Decomposition reactions of $NO_3$* and other adsorbed $NO_x$ species are discussed in more detail in the following two sections.

**Desorption and Reactions of Preadsorbed NO as a Function of Temperature.** Reactions of adsorbed NO during temperature ramping in He flow led to the evolution of unreacted NO and of $O_2$, $N_2O$, and small amounts of $N_2$ for all samples (Figures 7 and 8). These results are in qualitative agreement with previous studies on Cu−ZSM5 catalysts.[10,12,20−23] NO evolution occurs over a broad temperature range (300−750 K), as three broad peaks centered at about 380, 490, and 660 K on all catalysts, whereas $O_2$ desorbs as a single peak at higher temperatures (∼660 K). $N_2O$ forms at room temperature during NO adsorption on He-treated samples and desorbs also in two other peaks at 380 and 620 K (Cu(0.60), Figure 7). On samples treated in 50% $O_2$/He before NO chemisorption, only the two $N_2O$ peaks at elevated temperatures appear in substantial amounts, and the total amount of desorbed $N_2O$ (0.08 $N_2O$/Cu, Figure 8b) is smaller than for samples treated in He before contact with NO at ambient temperature (0.20 $N_2O$/Cu, Figure 8a). The larger amount of $N_2O$ formed on He-treated samples, which contain a larger number of reduced Cu dimers (*),[27] implicates such sites in the formation and reactions of adsorbed NO species, with the subsequent formation of O* after $N_2O$ desorption.

As expected from the larger fraction of Cu that appears as Cu dimers on Cu(0.60), the amount of $N_2O$ formed on this catalyst (0.22 $N_2O$/Cu) is larger than that on Cu(0.36) (0.20 $N_2O$/Cu). The similar desorption profiles for samples with a wide range of Cu/Al ratio suggest that similar Cu species are prevalent on these samples, albeit with different relative abundances. As a result, similar NO decomposition pathways,

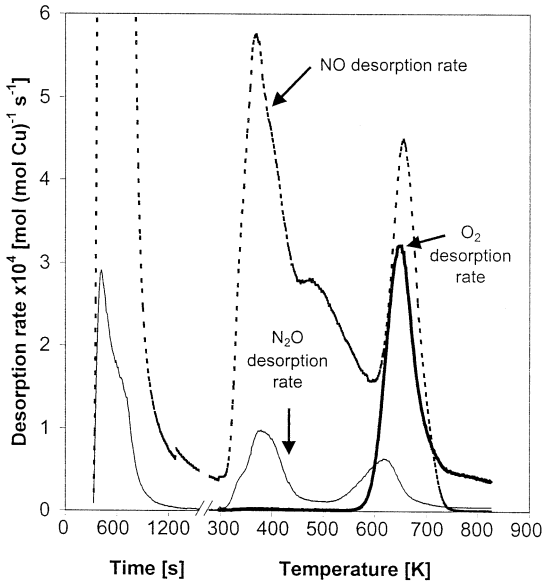


**Figure 7.** Evolution of products from preadsorbed NO during temperature programming in He carrier gas on Cu(0.60) treated in He at 773 K for 2 h before NO adsorption. $N_2O$ formation is shown during NO adsorption at 298 K. Zero in the time scale represents the time at which NO flow started. The temperature was ramped from 298 to 823 K at 0.167 K s$^{-1}$ after NO was removed from the gas phase [0.3 g, 1.67 cm$^3$ s$^{-1}$ total flow rate].

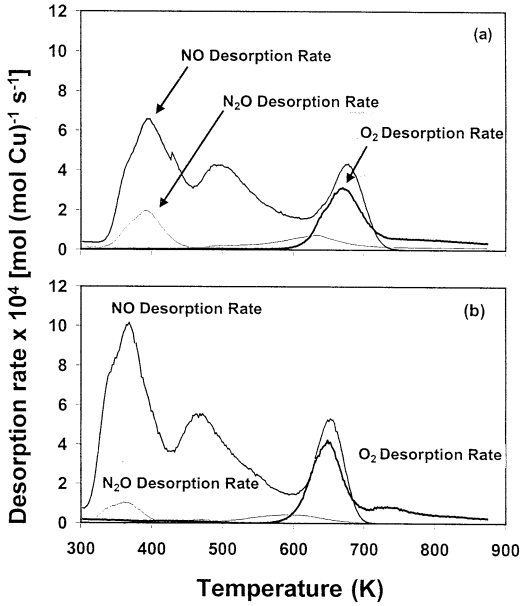


**Figure 8.** (a) Evolution of products from preadsorbed NO during temperature programming in He carrier gas on Cu(0.36) treated in He at 773 K for 2 h before NO adsorption. The temperature was ramped from 298 to 823 K at 0.167 K s$^{-1}$ [0.3 g, 1.67 cm$^3$ s$^{-1}$ total flow rate]. (b) Evolution of products from preadsorbed NO during temperature programming in He carrier gas on Cu(0.36) treated in 50% $O_2$/He at 773 K for 2 h before NO adsorption. The temperature was ramped from 298 to 823 K at 0.167 K s$^{-1}$ [0.3 g, 1.67 cm$^3$ s$^{-1}$ total flow rate].

but a varying number of active sites, are expected on these samples.[27]

At 298 K, NO adsorption leads to infrared bands for $Cu^+$-(NO) and $Cu^+(NO)_2$ on Cu−ZSM5 samples pretreated in He at 823 K.[5,16] These bands become less intense with increasing time in contact with NO, during which they are gradually replaced with bands assigned to $Cu^{2+}O^-$(NO). This oxidation of $Cu^+$ to $Cu^{2+}$ is consistent with the observed evolution of $N_2O$ from adsorbed NO near ambient temperature (Figure 7).

The evolution of $N_2O$ at ambient temperatures indicates that the activation energy for $N_2O$ formation is very low. Reduced Cu dimers (*) provide two vicinal NO adsorption sites, and such structures allow the formation of N−N bonds with low activation barriers. As discussed elsewhere,[26] this low activation energy, together with the significant adsorption enthalpy for NO on reduced Cu atoms within such dimers, leads to the negative apparent activation energy observed on Cu−ZSM5 catalysts at high temperatures.

The $N_2O$ desorption peak at 380 K (Figures 7 and 8) coincides with the first NO desorption peak, suggesting that $N_2O$ desorbs concurrently with some of the adsorbed NO. $Cu^+(NO)$ infrared bands become weaker at ∼373 K during steady-state NO decomposition.[16] Thus, it seems that isolated and unreactive $Cu^+(NO)$ species (NO*), adsorbed on one of the two $Cu^+$ atoms within a reduced dimer, become reactive as adsorbed NO becomes mobile during desorption and reequilibrates to form the two vicinal $Cu^+(NO)$ species required for N−N bond formation. The readsorption of NO as it desorbs and moves along the catalyst bed leads to the formation of some dimers with the required two NO molecules. As a result, NO and $N_2O$ appear simultaneously in the gas phase during these experiments (Figures 7 and 8). The steps involved are shown schematically in eqs 3−5, as previously suggested.[7]

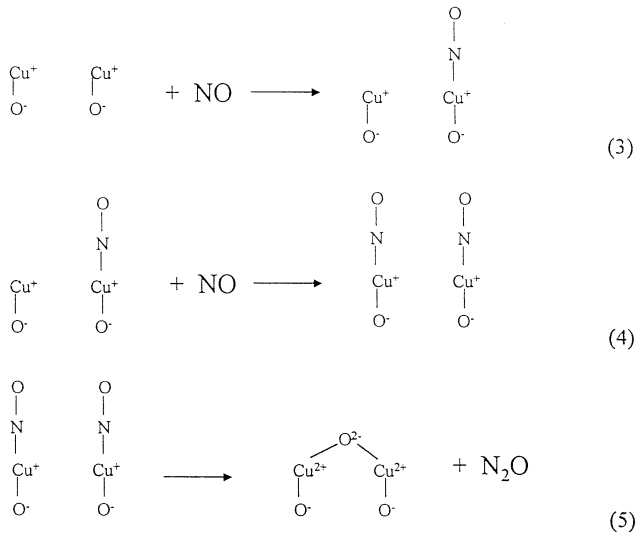


NO desorbs at 490 K without the concurrent evolution of any other species, indicating that NO does not react to form N−N bonds or $NO_2$ molecules via reactions with reduced or oxidized Cu dimers at these temperatures. The species responsible for this NO desorption peak appear to be spectators, distinct from those adsorbed on reduced Cu dimers.

The third $N_2O$ peak at ∼620 K is assigned to the readsorption of some of the NO desorbed at ∼490 K on Cu dimers that have been reduced by the process responsible for the incipient desorption of $O_2$ at ∼650 K. It is likely, as discussed below, that these sites are formed by reaction of NO with O* to form $NO_2$ (eq 6), which then readsorbs on other oxidized dimers to form $NO_3$* (eq 7). At these temperatures, $NO_3$* species are stable and most of the desorbed $NO_2$ molecules tend to readsorb on oxidized Cu dimers.

$O_2$ desorbs in a peak at 660 K, simultaneously with the last NO desorption peak. This simultaneous evolution of NO and $O_2$ indicates that they form via decomposition of a common intermediate. $NO/O_2$ molar ratios for these peaks are between 1 and 2, with the higher ratios observed on samples pretreated

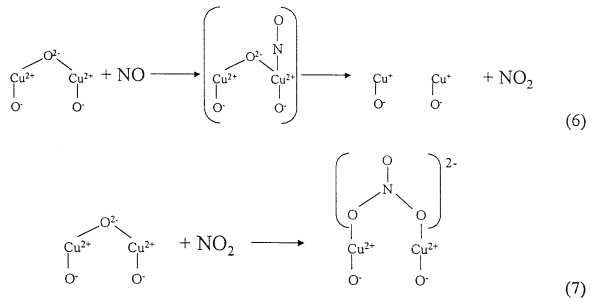


in He instead of 50% $O_2$/He. These $NO/O_2$ ratios are consistent with adsorbed $NO_3$, and these ratios reflect a mixture of Cu sites in their reduced (*) and oxidized (O*) states as end products, as shown in eqs 8 and 9, which would lead to ratios

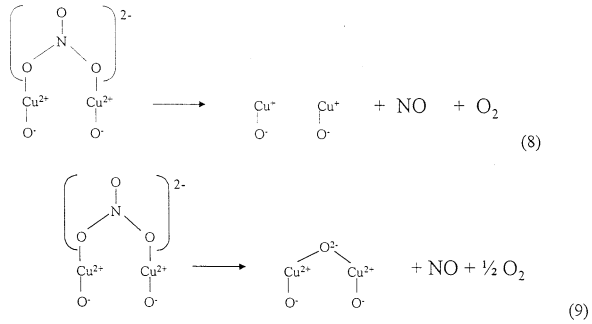


of 1 and 2, respectively. Equation 9 reflects the net decomposition of $NO_3$* to form O* and it is not necessarily an elementary step. $NO_2$ is the first desorption product in this sequence, but low concentrations of NO and $O_2$ and unfavorable thermodynamics lead to the catalytic decomposition of $NO_2$ into NO and $O_2$ via the reverse of step 6 and steps 7 and 8.

Above 700 K, $O_2$ desorbs in small amounts via the recombination of remaining O* sites. The $NO_3$ pathway for $O_2$ formation becomes unavailable for these O* sites because NO is no longer present in the contacting gas phase at these high temperatures. The infrared bands associated with $NO_3$* disappear around 673 K, without the detection of any bands for adsorbed NO.[12,18] This is consistent with the mechanism for the concurrent evolution of NO and $O_2$ at 660 K on Cu−ZSM5 proposed this study. These mechanistic conclusions have been confirmed by the results obtained from reactions of adsorbed NO in the presence of NO in the gas phase, as discussed in the next section.

**Desorption and Decomposition of Adsorbed NO Using NO-Containing Carrier Gas.** Here, we examine desorption and reactions of adsorbed NO as the sample temperature is increased in the presence of gas-phase NO. The results are shown in Figure 9 for Cu(0.58) pretreated in 50% $O_2$/He. At low temperatures, $N_2O$ is formed, as in the case of reactions of preadsorbed NO with He as a carrier gas. This sample shows detectable amounts of $N_2O$, even though reduced sites are not expected to remain after treatment at 773 K and cooling to ambient temperature in an $O_2$-containing stream. As shown in eqs 3−5 and previously proposed,[6,7] formation of $N_2O$ requires reduced Cu dimers.

One pathway for $N_2O$ formation on samples containing only oxidized dimers (O*) involves the reduction of dimers by NO to form $NO_2$ molecules (eq 6), which then readsorb on other oxidized dimers to form stable $NO_3$* species. The formation and desorption of $NO_2$ in the first step forms a reduced Cu dimer, which becomes available for adsorption and for sto-

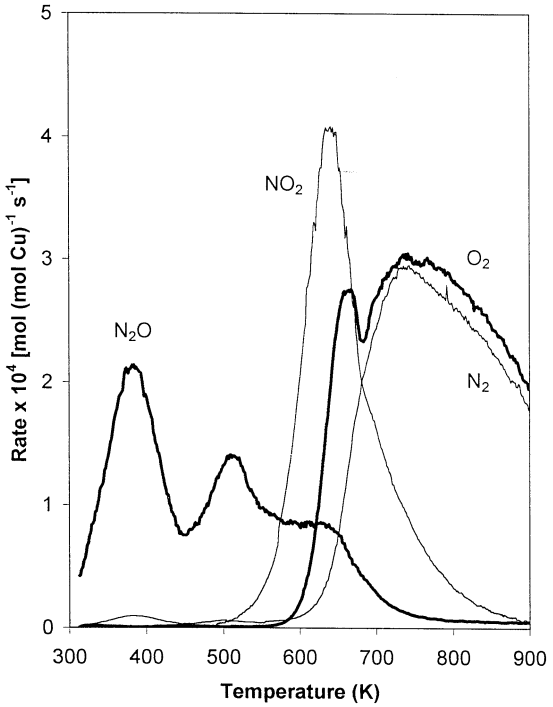


**Figure 9.** Rates of product evolution and NO molar rates in effluent during reactions of 0.464% NO/He on Cu(0.58) initially treated in 50% $O_2$/He at 773 K for 2 h. The temperature was ramped from 298 to 900 K at 0.167 K $s^{-1}$ [0.3 g, 1.67 $cm^3$ $s^{-1}$ total flow rate].

ichiometric decomposition of NO to $N_2O$ and O* near ambient temperatures (eq 5). The formation of $NO_3$* leads to the accumulation of a larger amount of oxygen than in fully oxidized fresh samples (1 vs 0.5 $O/Cu_{dimer}$ in addition to adsorbed NO). In this manner, the oxidation of NO to $NO_2$ allows the concurrent reduction of two NO molecules to one $N_2O$ molecule with the overall stoichiometry of eq 10.

$$O^* + 3NO \rightarrow NO_3^* + N_2O \qquad (10)$$

Another possibility for the accumulation of adsorbed oxygen species during formation of $N_2O$ on oxidized samples is the adsorption of $NO_2$, as previously suggested from infrared data.[6] NO could reduce $\{Cu^{2+}-O^{2-}-Cu^{2+}\}^{2+}$ dimers, leading to $Cu^+$-(NO) and to $NO_2$ adsorbed as a $(Cu-NO_2)^+$ complex near room temperature. However, these $NO_2$ species must desorb for two $Cu^+$(NO) species to coexist within a dimer and then react to form the observed $N_2O$ products. Therefore, although via a different sequence, this mechanism involves the same elementary steps for $N_2O$ formation as those described in the previous paragraph. The $NO_2$ desorbed is not detected in the effluent because it readsorbs at these low temperatures to form $NO_3$* on the predominant Cu structures (oxidized Cu dimers).

$N_2O$ formation rates ultimately decrease as the temperature increases above 373 K (Figure 9), even though NO reactants remain in the gas phase. No oxygen-containing products, except $N_2O$, are detected below 500 K; this indicates that oxygen must accumulate on the surface in the 300−500 K range, leading to a gradual increase in the oxygen content of the most abundant adsorbed species. As discussed above, these species are likely to be adsorbed $NO_3$* structures, which decompose only at higher temperatures. $N_2O$ formation decreases with increasing temperature because $NO_3$* species occupy most of the Cu dimer sites. These pathways provide a stoichiometric reaction for the formation of $N_2O$ (eq 10). The kinetic coupling of this reaction with $NO_3$* decomposition completes the catalytic cycle for NO decomposition by providing a pathway for net oxygen removal, but only at higher temperatures, which are required for $NO_3$* decomposition.

As the temperature increases above 500 K, large amounts of $NO_2$ desorb from the catalyst (0.27 $NO_2$/Cu) as $NO_3$* becomes unstable. At these temperatures quasi-equilibrium is achieved among $NO_2$, NO, and $O_2$ molecules in the gas phase.[26,29,30] Thermodynamics favor $NO_2$ at low temperatures; as a result, $NO_2$ is the predominant product of $NO_3$* decomposition at ∼623 K, whereas NO and $O_2$ are thermodynamically favored at higher temperatures (Figure 9). The amount of $NO_2$ formed in this experiment is much larger than that formed when He is used as the carrier gas (see previous section), because NO and $O_2$ concentrations are much higher when the carrier gas contains NO and this leads to higher equilibrium $NO_2$ concentrations.

$O_2$ evolution starts at ∼573 K and it reaches maximum rates at 670 K (Figure 9). These $O_2$ formation pathways are identical to those involved in the decomposition of preadsorbed NO in a He carrier. $O_2$ forms in this case, however, via both stoichiometric decomposition of adsorbed $NO_3$* and via catalytic decomposition of some of the NO present in the gas phase, which also involves a $NO_3$* decomposition step. At temperatures above those required for $NO_3$* decomposition (∼685 K), $N_2$ and $O_2$ evolve in nearly equimolar amounts via steady-state catalytic reactions of gas-phase NO molecules. A residual slight excess of $O_2$ in the effluent stream, however, indicates that net oxygen removal from these samples continues up to 923 K. This leads to an increasing concentration of $\{Cu^+-\square-Cu^+\}^{2+}$ species with increasing temperature, as suggested also by steady-state NO decomposition rate measurements.[26]

**Assessment of $O_2$ Formation Mechanism during Catalytic and Stoichiometric Reactions of NO.** The isothermal and nonisothermal transient data described above suggest that $O_2$ formation pathways involve NO molecules as oxygen carriers. These carriers allow kinetic communication among oxygen atoms present at distant Cu dimers, via the quasi-equilibrated formation and decomposition of $NO_2$. Indeed, the equilibrium $NO_2$ concentrations prevalent during steady-state catalytic NO decomposition at 673−873 K ensure that such pathways are sufficiently fast to equilibrate gas-phase and surface oxygen pools and to account for all of the $O_2$ desorbed during steady-state NO decomposition.[26]

These conclusions were confirmed by measuring the net rate of oxygen removal from Cu−ZSM5 samples during heating in the presence and absence of NO in the carrier gas (Figure 10). In the absence of NO ($O_2$ TPD), $O_2$ desorbs only via recombination of O* species associated with Cu dimers or, if present, with CuO clusters. This process requires two oxygen atoms to be sufficiently near to form O═O bonds, either because of their permanent proximate location as part of vicinal oxidized dimers or after surface or gas-phase diffusion of O-atoms at much higher temperatures. When NO is present in the carrier gas, both NO-mediated transport in the gas phase and O* recombination desorption pathways become possible; in this case, all Cu dimers become active in redox processes irrespective of whether they are located within or beyond atomic O−O distances from each other. When NO is present in the carrier gas, the net oxygen removal rate was estimated using eq 2. Figure 11 shows the cumulative change in oxygen surface coverage, estimated by integration of the data in Figure 10 with the assumption that samples initially contain one O per Cu dimer. This assumption was confirmed and the number of Cu dimers was estimated from $H_2$ and CO reduction experiments.[27]

The recombinative $O_2$ desorption profile observed using He as the carrier gas (Figure 10) shows two features, as reported

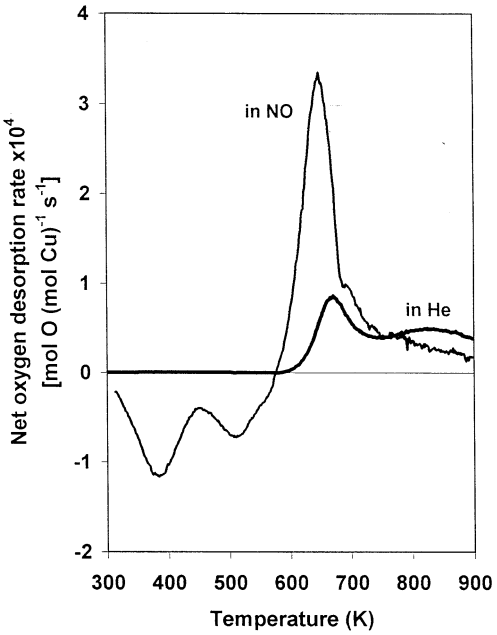


**Figure 10.** Net O evolution rates during reactions of 0.464% NO/He (labeled "in NO") and during desorption in He (labeled "in He") on Cu(0.58) treated in 50% $O_2$/He at 773 K for 2 h before desorption in He or NO reactions. The NO experiment is the same as the one presented in Figure 9.

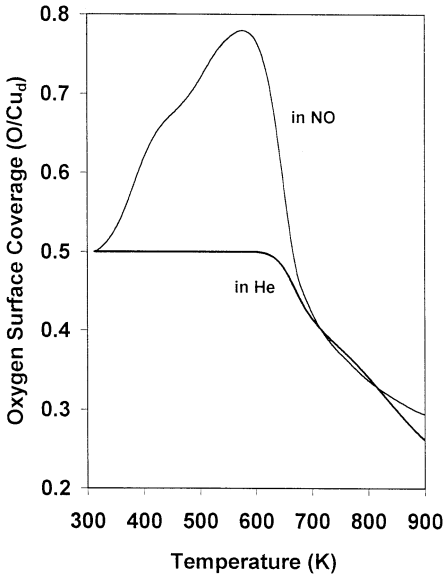


**Figure 11.** Oxygen surface coverage ($O/Cu_{dimer}$) relative to starting material for the same experiments as in Figure 10. The integration is started at 0.5 $O/Cu_{dimer}$.

also in a previous study.[24] A low-temperature peak at ~650 K appears to reflect vicinal oxygen-containing species, which would require minimal oxygen mobility for recombination events. This peak increases with increasing Cu/Al ratio, as expected from the decrease in the average distance among Cu dimers as the Cu content increases.[27] A broader peak at ~800 K is likely to require mobility of O*, Cu dimers, or even framework cations. Additional details about the $O_2$ desorption kinetics and the structure of Cu species in these materials are reported elsewhere.[27]

When NO molecules are present in the carrier gas, the oxygen content in Cu−ZSM5 increases as the sample temperature increases from 298 to 573 K, because of the formation of $NO_3$*, as mentioned in the previous section (Figure 11). Above ~573 K, $NO_3$* becomes unstable and decomposes according to eqs 8

**NO activation and $N_2O$ and $N_2$ formation**

| | | | | | | | |
|---|---|---|---|---|---|---|---|
| 1. | * | + | NO | ⇌ | NO* | | (quasi-equilibrated) |
| 2. | NO* | + | NO | ⇌ | $(NO)_2$* | | (quasi-equilibrated) |
| 3. | $(NO)_2$* | | | → | O* | + $N_2O$ | |
| 4. | * | + | $N_2O$ | ⇌ | $N_2O$* | | (quasi-equilibrated) |
| 5. | $N_2O$* | | | → | O* | + $N_2$ | |

**$O_2$ formation**

| | | | | | | | |
|---|---|---|---|---|---|---|---|
| 6. | O* | + | NO | ⇌ | $NO_2$* | | (quasi-equilibrated) |
| 7. | $NO_2$* | | | ⇌ | * | + $NO_2$ | (quasi-equilibrated) |
| 8. | O* | + | $NO_2$ | ⇌ | $NO_3$* | | (quasi-equilibrated) |
| 9. | $NO_3$* | | | ⇌ | $O_2$* | + NO | (quasi-equilibrated) |
| 10. | $O_2$* | | | ⇌ | * | + $O_2$ | (quasi-equilibrated) |

**Figure 12.** Proposed mechanism for NO decomposition on Cu−ZSM5.

and 9. This results in the net removal of oxygen atoms from the samples, the rate of which reaches a maximum value at ~623 K. The catalyst oxygen content in the NO-containing carrier gas then rapidly approaches that measured with pure He as the carrier gas and ultimately becomes slightly lower than the latter at ~700 K. Thus, even though O* is continuously formed during NO decomposition and the concentration of $O_2$ in the gas phase is much higher than with the pure He carrier gas, the oxygen content in the catalyst is lower when NO is present in the contacting gas phase. Clearly, the pathways available for oxygen removal are more effective when NO is present, as expected if NO were involved in facilitating $O_2$ formation via $NO_2$ formation−decomposition equilibrated pathways.

Above ~700 K, $NO_3$* coverages are negligible, and O* and * become the most abundant surface species in both the presence and absence of NO. When NO is present, $O_2$ and O* are in quasi-equilibrium (via the $NO_2$−NO redox reaction) and oxygen removal rates above 700 K are controlled by the temperature-dependent equilibrium constant for $O_2$ adsorption, which sets its concentration in the flowing gas.[26] With pure He as the carrier, O* is not formed continuously and $O_2$ formation rates are controlled by the kinetics of recombinative desorption. Thus, at high temperatures, Cu species from which O* has desorbed remain reduced with He as the carrier gas, while such reduced species are continuously reoxidized as part of redox cycles responsible for NO decomposition turnovers when NO is present in the gas phase. This explains why the oxygen content becomes comparatively lower in the absence of NO above 800 K (Figure 11).

We have shown that NO-mediated pathways for $O_2$ formation are more rapid than O* recombination to form $O_2$. These pathways also allow all Cu dimers to become potential active sites for NO decomposition, because such pathways do not require vicinal Cu dimers to complete catalytic turnovers via recombinative $O_2$ formation.

Our results are relevant also to the mechanism for $N_2O$ decomposition reactions on Cu−ZSM5[31−36] and Fe−ZSM5.[37−39] $N_2O$ is an intermediate in NO decomposition, and its ultimate decomposition to $N_2$ and $O_2$ is required in order to complete NO decomposition turnovers. Thus, NO and $N_2O$ decomposition reactions are mechanistically entangled. Both reactions require the stoichiometric formation of $O_2$, the mechanism of which is common to both reactions. Oscillatory $N_2O$ decomposition rates[31] have been attributed to the gradual accumulation and rapid decomposition of adsorbed nitrate species,[32,33] a conclusion recently confirmed by infrared studies.[36] On Cu−ZSM5[32] and Fe−ZSM5,[38,39] the presence of NO increases $N_2O$ decomposition rates. This "catalytic" effect of NO on $N_2O$ decomposition rates is consistent with the NO-mediated oxygen removal

pathways proposed here for NO decomposition, which render Cu dimers sites reducible and available for redox catalytic turnovers. The transient kinetic measurements proposed here and a companion study of steady-state NO decomposition kinetics[26] have led to a consistent set of elementary steps that can explain how NO decomposes into $N_2$, $N_2O$, $NO_2$, and $O_2$ on Cu−ZSM5 (Figure 12).

## Conclusions

Isothermal and nonisothermal transients were carried out during NO decomposition on Cu−ZSM5 catalysts in order to examine the nature of the required redox cycles, reactive intermediates, and active sites. These experiments involved the measurements of the dynamic evolution of desorption and reaction products (NO, $N_2O$, $NO_2$, $N_2$, and $O_2$) during reaction in order to obtain information about the mechanism of NO decomposition. $N_2$ formation rates were proportional to the number of reduced centers $\{Cu^+-\square-Cu^+\}^{2+}$, and they decreased as the number of these centers decreased during a switch from He to 0.464% NO/He streams. An isothermal switch from 1% NO/He to He at 673 K led to an increase in net $O_2$ formation rates immediately after the switch, indicating that NO mediates the removal of oxygen from nonvicinal $\{Cu^{2+}-O^{2-}-Cu^{2+}\}^{2+}$ dimers via the formation of $NO_2$* and $NO_3$* species. These species are also intermediates in the established quasi-equilibrium between NO, $O_2$, and $NO_2$. $NO_3$* species are stable up to ~573 K but decompose into NO and $O_2$ at higher temperatures, thus providing rapid pathways for $O_2$ formation, which, in contrast with recombinative desorption steps, do not require vicinal $\{Cu^{2+}-O^{2-}-Cu^{2+}\}^{2+}$ dimers.

These findings are consistent with some of the previously reported mechanistic details for this reaction, but they provide a more complete picture than previously available, including the critical oxygen removal pathways, previously attributed to recombinative desorption. The proposed sequence of elementary steps contains as an intrinsic component the pathways required for the decomposition of $N_2O$, which occurs as a sequential reaction during NO decomposition.

**Acknowledgment.** B.M. acknowledges a grant from CF Miljöfonden and P.D. a grant from the French Foreign Affairs Ministry under the "Programme Lavoisier". D.K.L. acknowledges the support of the Korea Science and Engineering Foundation (KOSEF).

## References and Notes

(1) Iwamoto, M.; Yokoo, S.; Sakai, K.; Kawaga, S. *J. Chem. Soc., Faraday Trans*. **1981**, *77*, 1629.
(2) Iwamoto, M.; Furukawa, H.; Mine, Y.; Uemura, F.; Mikuriya, S.; Kagawa, S. *J. Chem. Soc., Chem. Commun.* **1986**, *16*, 1272.
(3) Iwamoto, M.; Yahiro, H.; Mine, Y.; Kagawa, S. *Chem. Lett.* **1989**, *2*, 213.
(4) Iwamoto, M.; Yahiro, H.; Tanda, K.; Mizuno, N.; Mine, Y.; Kagawa, S. *J. Phys. Chem*. **1991**, *95*, 3727.
(5) Iwamoto, M.; Yahiro, H.; Mizuno, N.; Zhang, W. X.; Mine, Y.; Furukawa, H.; Kagawa, S. *J. Phys. Chem*. **1992**, *96*, 9360.
(6) Beutel, T.; Sarkany, J.; Lei, G. D.; Yan, J. Y.; Sachtler, W. M. H. *J. Phys. Chem.* **1996**, *100*, 845.
(7) Lei, G. D.; Adelman, B. J.; Sarkany, J.; Sachtler, W. M. H. *Appl. Catal. B* **1995**, *5*, 245.
(8) Li, Y.; Hall, W. K. *J. Catal.* **1991**, *129*, 202.
(9) Schay, Z.; Guczi, L. *Catal. Today* **1993**, *17*, 175.
(10) Schay, Z.; Kiricsi, I.; Guczi, L. *Stud. Surface Sci. Catal.* **1998**, *116*, 347.
(11) Schay, Z.; Knozinger, H.; Guczi, L.; Pal-Borbely, G. *Appl. Catal. B* **1998**, *18*, 263.
(12) Konduru, M. V.; Chuang, S. S. C. *J. Phys. Chem. B* **1999**, *103*, 5802.
(13) Spoto, G.; Zecchina, A.; Bordiga, S.; Ricchiardi, G.; Martra, G.; Leofanti, G.; Petrini, G. *Appl. Catal. B* **1994**, *3*, 151.
(14) Giamello, E.; Murphy, D.; Magnacca, G.; Shioya, Y.; Nomura, T.; Anpo, M. *J. Catal.* **1992**, *136*, 510.
(15) Valyon, J.; Hall, W. K. *J. Phys. Chem.* **1993**, *97*, 1204.
(16) Aylor, A. W.; Larsen, S. C.; Reimer, J. A.; Bell, A. T. *J. Catal.* **1995**, *157*, 592.
(17) Konduru, M. V.; Chuang, S. S. C. *J. Catal.* **1999**, *187*, 436.
(18) Konduru, M. V.; Chuang, S. S. C. *J. Catal.* **2000**, *196*, 271.
(19) Jang, H.-J.; Hall, W. K.; d'Itri, J. L. *J. Phys. Chem*. **1996**, *100*, 9416.
(20) Li, Y.; Armor, J. N. *Appl. Catal*. **1991**, *76*, L1.
(21) Adelman, B. J.; Lei, G. D.; Sachtler, W. M. H. *Catal. Lett.* **1994**, *28*, 119.
(22) Chang, Y.; McCarty, J. G. *J. Catal.* **1997**, *165*, 1.
(23) Gervasini, A. *Appl. Catal. B* **1997**, *14*, 147.
(24) Valyon, J.; Hall, W. K. *J. Catal.* **1993**, *143*, 520.
(25) Trout, B. L.; Chakraborty, A. K.; Bell, A. T. *J. Phys. Chem.* **1996**, *100*, 17582.
(26) Moden, B.; Da Costa, P.; Fonfe, B.; Lee, D. K.; Iglesia, E. *J. Catal.* **2002**, *209*, 75.
(27) Da Costa, P.; Moden, B.; Meitzner, G. D.; Lee, D. K.; Iglesia, E. *Phys. Chem. Chem. Phys.*, in press.
(28) Boudart, M.; Djega-Mariadassou, G. In *Kinetics of Heterogeneous Catalytic Reactions*; Princeton University Press: Princeton, NJ, 1984.
(29) Petunchi, J. O.; Hall, W. K. *Appl. Catal. B* **1993**, *2*, L17.
(30) Shelef, M.; Montreuil, C. N.; Jen, H. W. *Catal. Lett.* **1994**, *26*, 277.
(31) Lintz, H. G.; Turek, T. *Catal. Lett.* **1995**, *30*, 313.
(32) Turek, T. *Appl. Catal. B* **1996**, *9*, 201.
(33) Turek, T. *J. Catal.* **1998**, *174*, 98.
(34) Ciambelli, P.; Di Benedetto, A.; Garufi, E.; Pirone, R.; Russo, G. *J. Catal.* **1998**, *175*, 161.
(35) Kapteijn, F.; Marban, G.; Rodriguez-Mirasol, J.; Moulijn, J. A. *J. Catal.* **1997**, *167*, 256.
(36) Fanson, P. T.; Stradt, M. W.; Delgass, W. N.; Lauterbach, J. *Catal. Lett.* **2001**, *77*, 15.
(37) El-Malki, El-M.; van Santen, R. A.; Sachtler, W. M. H. *J. Catal.* **2000**, *196*, 212.
(38) Sang, C.; Lund, C. R. F. *Catal. Lett.* **2001**, *73*, 73.
(39) Mul, G.; Perez-Ramirez, J.; Kapteijn, F.; Moulijn, J. A. *Catal. Lett.* **2001**, *77*, 7.